Astron. Astrophys. 343, 466–476 (1999)

ASTRONOMY
AND
ASTROPHYSICS

# Modelling the spectral energy distribution and SED variability of the Carbon Mira R Fornacis⋆

**A. Lobel**[1], **J.G. Doyle**[1], **and S. Bagnulo**[2]

[1] Armagh Observatory, College Hill, Armagh BT61 9DG, Ireland
[2] Institut für Astronomie, Universität Wien, Türkenschanzstrasse 17, A-1180 Wien, Austria

Received 2 July 1998 / Accepted 2 December 1998

**Abstract.** We have developed a new method to determine the physical properties and the local circumstances of dust shells surrounding Carbon- and Oxygen-rich stars for a given pulsation phase. The observed mid-IR dust emission feature(s), in conjunction with $IRAS$ BB photometry and coeval optical and near-IR BB photometry, are modelled from radiative transport calculations through the dust shell using a grid of detailed synthetic model input spectra for M-S-C giants. From its application to the optical Carbon Mira R For we find that the temperature of the inner shell boundary exceeds 1000 K, ranging between 1200 K and 1400 K. The optical depth of the shell at 11.3 $\mu$m is determined at $\tau_{11\,\mu m}$=0.105 with $T_{\rm eff}$=3200$\pm$200 K for the central star in the considered phase of variability. By-products of the analysis are the shell composition of 90% amorphous carbon and only 10% SiC grains with rather small average radii of 0.05$\pm$0.02 $\mu$m. The dust density distribution assumes a power law of $r^{-2}$ for a steady-state wind with a geometrical thickness ranging between $10^4$ and $5\,10^4$ times the inner boundary shell radius and with a high gas mass-loss rate of 3–4 $10^{-6}\ M_\odot\ {\rm y}^{-1}$ derived by radiation pressure onto the dust. We show that the optical and near-IR light curves are strongly affected by small changes of $T_{\rm eff}$ and of the shell optical depth with pulsation. A comparison of high resolution optical spectra of R For and medium/low resolution spectra of other carbon stars with the selected model input spectrum is also provided.

**Key words:** stars: AGB and post-AGB – stars: mass-loss – stars: individual: R For – stars: carbon

## 1. Introduction

The presence of grain shells around C- and O-rich stars is studied already for several decades, and early spectroscopic and photometric detections of excess emission from optically thin circumstellar dust near these evolved variables date back to the late 1960 s (Treffers & Cohen 1974). These spectral 'features', often observed for instance at 11.3 $\mu$m, are attributed to silicon-carbide (SiC) grains around stars with carbon-rich atmospheres, whereas a feature seen near 9.7 $\mu$m is ascribed to silicate grains in the environments of O-rich stars. Low resolution spectra of Asymptotic Giant Branch (AGB) stars observed by *IRAS* in the mid-1980 s enabled a classification of these features (Little-Marenin & Little 1988) and to attempt the modelling of their formation conditions. To that end various sophisticated numerical codes have been developed since. A brief review of their gradual improvements over the years and a performance comparison of three modern codes was discussed by Ivezić et al. (1997), currently including direct solutions for the pure scattering problem in their publicly available DUSTY code. Their method is based on exact solutions of a self-consistent equation for the radiative energy density, including dust scattering, absorption and emission in spherical shell geometry (Ivezić et al. 1996). From an application to *IRAS* Low Resolution Spectrograph (LRS) spectra and colours of late-type stars they computed mass-loss rates by radiatively-driven outflows which are in agreement with other methods within a factor of two, and emphasised that the SiC (and silicate) features are formed at the inner parts of the dust envelopes for SiC abundances below 20%-30% in mixtures with amorphous carbon (Ivezić & Elitzur 1995). Bagnulo et al. (1998) have modelled the SED of 12 carbon stars with optically thin dust shells from optical, near-IR and *IRAS* broadband (BB) photometry and *UKIRT* mid-IR spectro-photometry of the dust emission. They applied an adapted radiative transfer code originally due to Haisch (1979), however without the self-consistent coupling with the equation of motion as incorporated in DUSTY (Netzer & Elitzur 1993). Nevertheless, all the dust- and SED-modelling available to date from these numerical codes, which do account for this coupling, is based on an assumption of a blackbody distribution of the stellar radiation. For these cool atmospheres strong flux differences between the stellar continuum and the emerging atmospherical flux occur from molecular opacity sources (H, C, N, O compounds). These differences of the flux distribution from the central star, after being reprocessed through the dust shell, strongly affect the resulting SED from which the shell properties are to be derived. Therefore we presently determine the shell conditions for one target C-star, R Fornacis, using a grid of available synthetic input spectra to the DUSTY code.

*Send offprint requests to*: A. Lobel (ajrl@star.arm.ac.uk)

⋆ Based on observations taken at *UKIRT*, *CST*, *JCMT*, *SAAO*, *AAO* and the *IRAS* Pointsource Catalogue

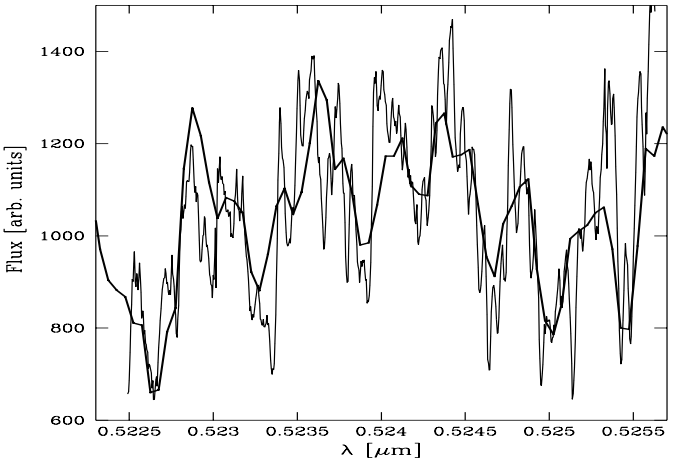


**Fig. 1.** The high-resolution spectrum of R For (C4) (thin line) strongly matches a medium-resolution spectrum of HD 223392 (C3) (bold line), indicating $T_{\rm eff} \geq 3000$ K

## 2. R Fornacis (AFGL 337)

From a study of mid-IR light curves Le Bertre (1992) observed a decreasing amplitude of variations with wavelength from about $1^{\rm m}.26$ in the $J$ band to $0^{\rm m}.57$ in the $N$ filter, further levelling off to $0^{\rm m}.32$ in $Q0$. Barthès et al. (1996) studied light curves of this long period variable ($P$=388 d.) and found decreasing amplitudes of the Fourier components from the visible to the near-IR and proposed a modulation of the light curves by the dust shell. Its average visual magnitudes at minimum and maximum brightness are $8^{\rm m}.9$ and $12^{\rm m}.2$, with occasionally extreme values of $7^{\rm m}.5$ and $13^{\rm m}.0$.

Earlier studies of R For by Feast et al. (1984) and by Le Bertre (1988) showed that an increased obscuration could result from condensation of grains in the inner portion of a circumstellar dust shell. In a study of 23 carbon-rich stars Le Bertre (1997) modelled the SED of R For from *IRAS* BB photometry and coeval optical and near-IR BB photometry. He adopted a blackbody temperature for the central star of 2600 K and obtained good fits to the *IRAS* photometry, but which clearly overestimated the optical photometry.

R For displays a rather weak SiC emission feature at 11.3 $\mu$m as observed by *IRAS* ('83) and by Speck et al. (1997) at *UKIRT* in '93. Our *UKIRT* spectrum between 16 and 24 $\mu$m was obtained on Aug. 22 '95 and the optical *BVRI* photometry at *SAAO* on Sept. 25 '95. The near-IR *JHKL′* photometry was obtained at *CST* (Tenerife) in early Sept. '95 (JD 2449967). For our accurate modelling of the SED and the dust emission feature we combine this data with another *UKIRT* spectrum taken between 8 and 13 $\mu$m and obtained in July '95. The difference of absolute flux at 11 $\mu$m between these three spectra is outside the calibration errors and within the amplitude changes in the $N$ filter (see further Sect. 3.2). These continuum humps show however no appreciable changes of shape with respect to the local background level. Changes in the shapes of silicate features of late-type stars have only recently been investigated and are proposed to result from varying optical dust properties with stellar pulsation. Likewise, several objects like V Hya and CIT 6, having rather weak dust emission features, display no apparent changes in shape with changing intensity (Monnier et al. 1998).

In Sect. 3 we describe the new modelling method of the SED of R For by means of the optical and near-IR BB photometric data of Sept. '95, together with the dust emission spectra observed in Jul.-Aug. '95. The SED variability during this phase is discussed in Sect. 4 using BB photometric data observed by Whitelock et al. (1997) between Aug. '95 and Jan. '96. This period follows a particular deep minimum about 1100 days earlier with clearly redder colours. Whitelock (1997) suggested RCB-type fadings, possibly linked with dust formation events. They however stress that there is no clear sign of periodicity in the obscuration events of R For and that the pre-whitened (removing the dominant period from the data) light curves are *not* periodic.

## 3. Modelling results

### *3.1. Selection of the atmospherical model*

The input model to the DUSTY code was selected from a grid of cool giant atmospherical models with $2200\,{\rm K} \leq T_{\rm eff} \leq 3800\,{\rm K}$, $-1.0 \leq \log(g) \leq 0.5$, $0.27 \leq$ C/O $\leq 1.02$ (by number) for $L_*$=10000 $L_\odot$, which was released by Allard et al. (1995). The resolution up to 2.5 $\mu$m is 2 Å and 5 Å up to 5 $\mu$m. The resolution then lowers to 0.1 $\mu$m up to 15 $\mu$m and is only 0.5–1 $\mu$m up to 90 $\mu$m. The models include opacities from important diatomic absorbers like CO, $C_2$, $C_3$, CN, CH, NH, MgH, butalso compounds like HCN, $C_2H_2$, TiO, SiO, SiH. For a description of the equation of state and the radiative transfer in spherical geometry and hydrostatic equilibrium with the PHOENIX code see Hauschildt et al. (1997) and Allard & Hauschildt (1995).

R For has been classified as C4,3e, but this information is insufficient to determine its atmospherical parameters, since the problem of spectral classification of C stars is to be considered still open. For instance, Alksne & Ikaunieks (1981, and references therein) give $T_{\rm eff}$ values of 4500 K for subclass C0 which fall to 3000 K for subclass C5. By contrast, Cohen (1979) gives 2900 K for a C4 star. In order to estimate the stellar parameters of R For, we have used high-resolution spectra offered in Barnbaum (1994). These echelle spectra only provide relative fluxes and can therefore not easily be compared with the absolute fluxes of the model spectra over a broad wavelength range. However, a comparison with a medium-resolution spectrum of another carbon star HD 223392 (C3,2), kindly provided by Dr. Andrews (1998, priv. comm.), and a low-resolution spectrum of HD 223392 obtained by Barnbaum et al. (1996) reveals that the model parameters of both stars are similar. It can be seen in Fig. 1 that the relative fluxes of HD 223392, resulting from strong atomic line blending (overlaid with vibration-rotational transitions of $C_2$ and CN), strongly match the high-resolution spectrum of R For, in which the individual atomic line cores are resolved.

We have then compared the strength of the broad molecular Swan $^{12}C_2$ bands (band heads shown in Fig. 2 at 4737 Å and 5165 Å) of HD 223392 with the grid of models having a carbon-to-oxygen ratio of 1.02 (and C, N, O number fractions

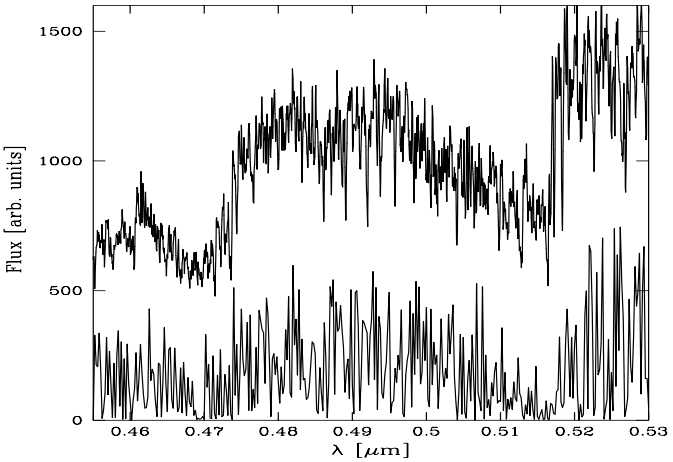


**Fig. 2.** The relative strength of the Swan $^{12}C_2$ bands in HD 223392 (bold line shifted upwards) compare best with these strengths in the synthetic input spectrum with $T_{\rm eff}$=3200 K and log(g)=0.0 (thin drawn line)

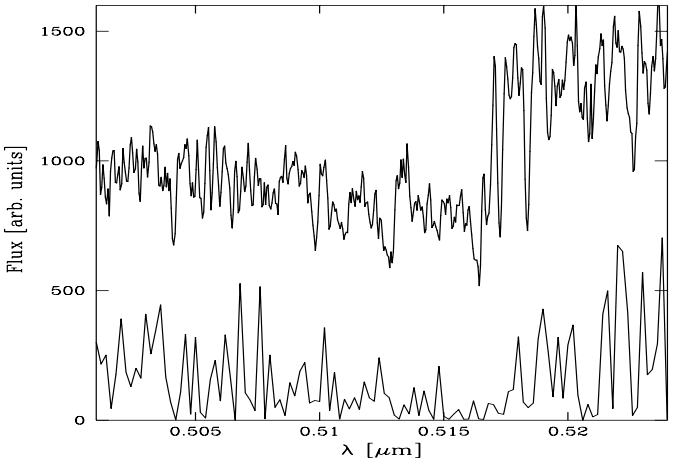


**Fig. 3.** The relative line intensities observed with medium resolution in HD 223392 (bold line shifted upwards) compare best to the synthetic model with $T_{\rm eff}$=3200 K, shown here in the $C_2$ bandhead at 5165 Å (thin line)

of resp. $6.8767\,10^{-4}$, $8.4874\,10^{-5}$ and $6.7418\,10^{-4}$, where the C abundance relative to the Sun is increased by a factor of 2.13). These bands attain maximum strength in C5–6 stars and decline rather sharply thereafter.

By means of a least-square technique we found that the best-fit to the observations is given by the model with $T_{\rm eff}$ = 3200 K and log(g)=0.0. We emphasize that the determination of these parameters results from finding a best fit to the overall observed SED and the flux at 11.3 $\mu$m. We found that adopting model atmospheres with lower $T_{\rm eff}$ as input to the DUSTY code could not reproduce the shape of the overall observed SED and the flux at the dust emission feature.

We have also checked that the Na $D$ lines in the high-resolution spectrum of R For are observed not to be intensity saturated. In the carbon input model with low $T_{\rm eff}$=2500 K the doublet is strongly saturated and the model temperature has to be increased to 3200 K in order to reduce the gas pressure and the resulting damping widths. But caution is needed when comparing relative strengths of saturated spectral features in order to check or estimate atmospheric parameters. This can be observed in Fig. 3 where an absorption blend around 0.521 $\mu$m in the selected model appears too strong when compared with the observed fluxes.

It should be noted that other authors have used lower values of $T_{\rm eff}$ in modelling the SED of R For ($T_{\rm eff}$=2500 K is commonly adopted). This discrepancy is likely to be due to the difference of applying an actual model spectrum or a blackbody for the stellar input spectrum. It appears in Fig. 4 that the model atmosphere with $T_{\rm eff}$ = 3200 K peaks at longer wavelengths than its corresponding blackbody. Since we find that this input model reproduces the observed SED of R For, it follows that instead by assuming a blackbody curve as model atmosphere, one is lead to adopt a lower value for the effective temperature.

For synthetic spectra with log(g)=0.5 there are no discernible differences with the overall absorption spectrum for log(g)=0.0, however there are minor differences in the optical

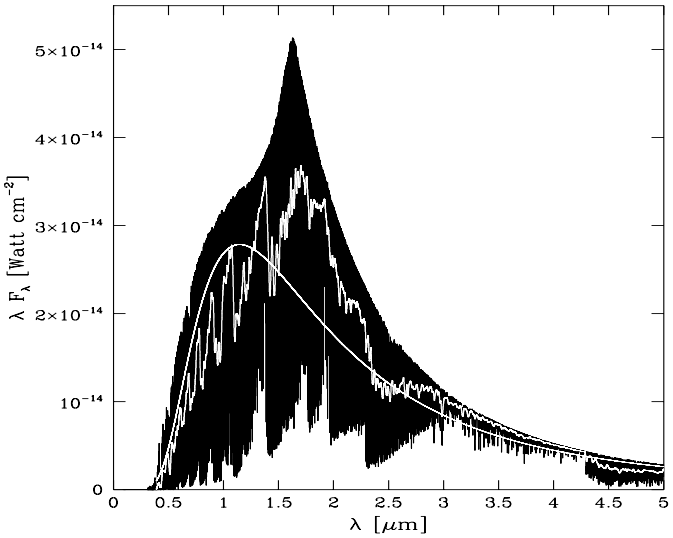


**Fig. 4.** The detailed input model spectrum (black) is smoothed by preserving the broad molecular bands (white curve). Note the considerable flux differences with its continuum blackbody ($T$=3200 K, smooth white curve) which strongly affects the SED when reprocessed by the dust envelope

flux levels. In the long-wave tail the shape of the model spectra follows the shape of the Planck function, although small differences with the continuum fluxes are present.

### *3.2. Overall method*

We have adapted the DUSTY code by increasing the predetermined wavelength grid of 98 to 468 wavelength points. As the model input spectra are too detailed to perform the radiative transfer within acceptable run times, the models are smoothed with total flux conservation between 0.1 and 5 $\mu$m (Fig. 4). This smoothed spectrum is then sampled onto 400 wavelength points in order to reassure that the broad molecular absorption bands

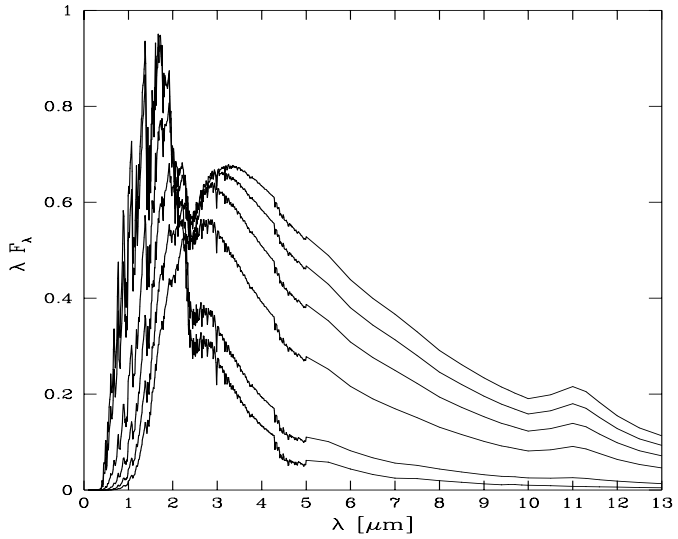


**Fig. 5.** The model spectrum (bold curve) is reprocessed by DUSTY and shown for 5 increasing optical depths of the dust shell; $\tau_{11} = 0.01, 0.05, 0.105, 0.15$ and 0.2 (thin curves upward). As $\tau_{11}$ increases the energy at shorter wavelengths is more reprocessed to the IR, resulting in stronger SiC emission at 11.3 $\mu$m

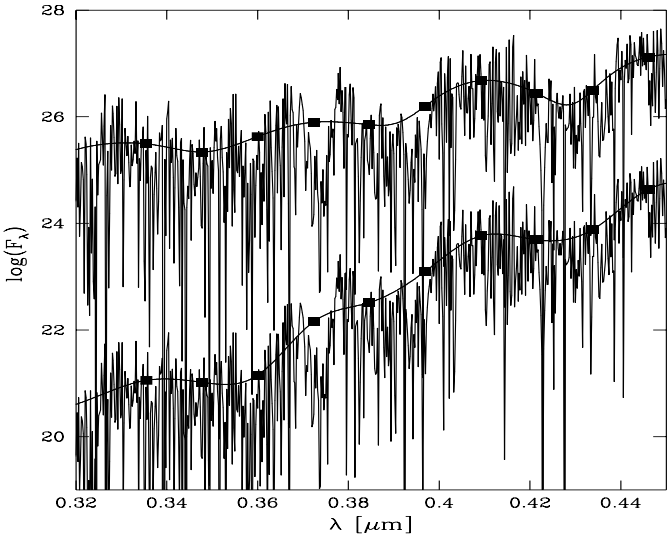


**Fig. 6.** The stellar model spectrum is smoothed (upper bold line) and reprocessed (lower bold line) at 468 wavelength points (boxes). The detailed output spectrum (lower thin line) is computed from the ratio of the cubic spline functions through these points with respect to the detailed input spectrum (upper thin line). This technique preserves the strong molecular and atomic line blanketing which affects the BB photometry of these cool giants

are preserved in the spectrum. The spectral tail beyond 5 $\mu$m is sampled onto 68 points, but somewhat more refined between 9 and 12 $\mu$m in order to model the shape of the dust emission feature(s). Next we compute a grid of reprocessed smoothed spectra for various shell parameters for a limited number of input models. A set of 5 spectra reprocessed from the input model with $T_{\rm eff}$=3200 K is shown in Fig. 5 for an optical thickness of the dust shell ranging from 0.01 to 0.2. As the optical depth increases the SiC feature at 11.3 $\mu$m becomes more pronounced and has higher intensity, whereas the optical flux levels decrease and the molecular bands weaken. Convergence is achieved at 95% total flux conservation for all output spectra, with run times ranging form 20 min. (on DEC Alpha) up to several hours for $\tau_{11} \geq 1$.

Detailed output spectra are subsequently constructed as follows. The 468 reprocessed and corresponding input fluxes are interpolated by cubic spline functions. Their ratio with respect to the detailed model input spectrum then provides the detailed output spectrum (Fig. 6). This opacity sampling technique allows one to preserve the overall energy redistribution and scattering by the CDS and its effect on the broadband filters. Note that the reprocessed model spectrum shown here should not be considered to represent detailed observed spectra as we expect that the CDS also blurs the spectral lines. But in the current approach we are mainly interested to account for the molecular and atomic line blanketing after being reprocessed by the dusty envelope. Doppler shifts of lines in the output spectrum due to the envelope expansion are expected to assume as much as a few angstroms and are hence negligible when compared to the width of these broad pass-bands.

Thereafter the reprocessed spectra are convoluted with the transmission functions in the *UBV* $(RI)_{\rm c}$, *JHKL′MN* and *IRAS*

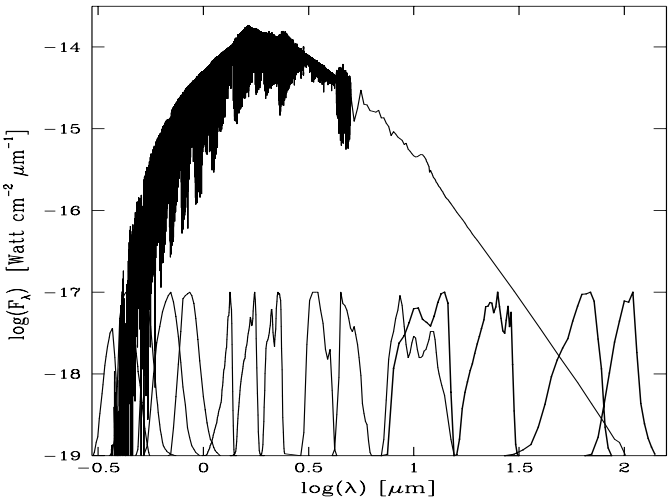


**Fig. 7.** The detailed reprocessed spectra are convoluted with 11 transmission functions of the *UBV*$(RI)_{\rm c}$*JHKL'MN* pass-bands (thin drawn filter shapes are shown scaled) and the 4 *IRAS* filters (bold shapes), producing 'synthetic' BB photometry

12, 25, 60 and 100 $\mu$m pass-bands (Fig. 7). The $B$, $J$ and $H$ bands are strongly affected by $C_2$ and/or CN. This has profound consequences when transforming magnitudes in absolute fluxes, and also when comparing observations obtained in similar – but not identical – photometric systems. For instance, our near-IR observations taken at *CST* appear to be not entirely consistent with those obtained by Whitelock et al. (1997) at *SAAO* in the same period (see further Table 2). This is fully explained by the different transmission functions of the two photometric systems. A convolution of our model SED with the $J$ band of the *CST*

system (Alonso et al. 1994) and with the $J$ band of the Johnson system (Landolt-Börnstein 1982) shows that the expected values for $J$ in the *CST* system are about $0^{\rm m}.33$ lower than in the Johnson system. Le Bertre (1997) noted that the $K$ band is not affected by CN and CO but also $L'$ is not affected by $C_2$ and HCN, and give therefore good estimates of the stellar continuum of carbon stars.

A best model is then selected from the computed grid by a least-squares method applied on the computed 'synthetic' BB photometry and the observed BB photometry, in conjunction with the best fit onto the observed dust emission feature. Note that the optical and near-IR data were corrected for interstellar extinction and the *IRAS* photometry for cirrus contamination as discussed in Bagnulo et al. (1998). When assuming a luminosity of $10000\,L_{\odot}$, we compute from the observed bolometric flux of $3.8\,10^{-7}\,{\rm erg\,s^{-1}cm^{-2}}$ a distance to R For of 0.93 kpc. The latter value is consistent with the observed HIPPARCOS parallax, which provides a distance in the range of 0.200–1.3 kpc. We then calculate an interstellar extinction in the $V$ band of $0^{\rm m}.20$ with the $A_{\rm v}$ equation of Milne & Aller (1980). Also Groenewegen et al. (1998) estimated only $0^{\rm m}.1$ for $l$=215.8 and a high galactic latitude $b$=−68.1. Note that Whitelock et al. (1997) find values as low as $0^{\rm m}.01$ from the Galactic extinction law by Feast et al. (1990). Below we discuss in more detail more aspects of the SED modelling.

### *3.3. Optical depth*

In the case of R For we find that the optical depth (considered here at a reference wavelength of 11.3 $\mu$m) of the dust shell cannot be constrained from a best fit onto the absolute flux of the dust emission feature alone. This results from the rather small dust optical depth and therefore a 'best' fit for a given $\tau_{11}$ and $T_{\rm eff}$ value can always be obtained when both parameters are altered oppositely over a confined range. This is because for limited changes of $T_{\rm eff}$ the slope of the output spectrum hardly changes in the 8 to 24 $\mu$m window. $\tau_{11}$ and $T_{\rm eff}$ can therefore only be fixed by considering the entire SED together with the intensity of the dust emission. In Fig. 8 it is shown that the shell optical depth is strongly constrained by the optical data. Slight variations in the dust opacity (or column density) strongly affect the emerging optical fluxes. A comparison between the reprocessed flux distribution and the observations strongly fixes $\tau_{11}$ at 0.105 (or $\tau_1$ =1.91 at 1 $\mu$m) and the $T_{\rm eff}$ of the input model around 3200±200 K. The spectral shape derived from a model with $T_{\rm eff}$=2500 K could not be reconciled with the observed SED and flux at 11.3 $\mu$m. We point out clearly here that excellent fits to the SiC feature can be obtained from input blackbody distributions for example as low as $T_{\rm eff}$=2200 K and $\tau_{11}$=0.057 when omitting the modelling of the entire SED (see Fig. 9). The flux differences between the blackbody and the actual atmospherical model, in particular at the shorter wavelengths, result in considerably different flux levels when reprocessed by the dust shell as the bolometric flux must remain conserved.

The determination of the shell composition for R For is independent of the multi-dimensional parameter search problem.

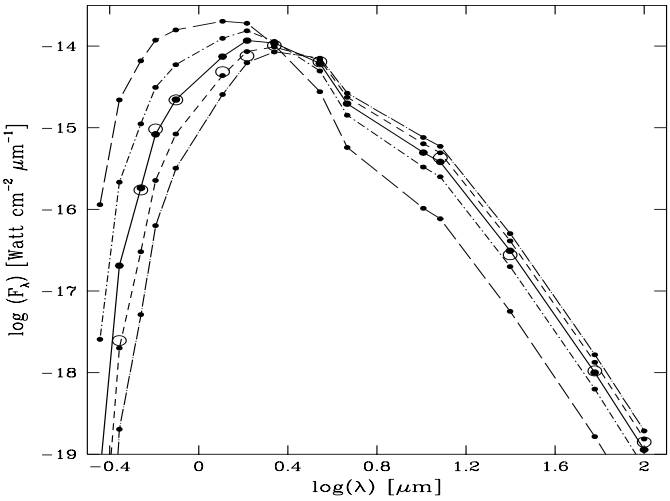


**Fig. 8.** The parameters of the dust shell are determined by a least-squares search on the synthetic and observed BB data of R For (open circles), in conjunction with a best fit onto the dust emission feature. A best fit is obtained for $\tau_{11}$=0.105 (bold solid curve), which is strongly constrained by the fit to the optical BB data. The other curves are computed for $\tau_{11}$=0.01 (long dashed), 0.05 (short-dash dotted), 0.15 (short dashed) and 0.2 (long-dash dotted)

Since the dust shell is rather optically thin, the shape of the SiC feature and its intensity against the background is practically independent of the optical depth, as is shown in Fig. 9. If the shell were optically thicker and a change of $\tau_{11}$ would strongly influence the shape of the feature, the parameter search would become much more involved, and possibly under-defined. We obtain a best fit to the dust emission feature for only 10±5% SiC grains and 90±5% amorphous carbon (amC) (Fig. 9 lower panel). The optical properties of $\alpha$-SiC and the amC background are respectively taken from Pégourié (1988) and Hanner (1988) (see also Zubko et al. 1996 or Rouleau & Martin 1991), and were supplied to DUSTY after interpolating them for our extended grid of 468 wavelength points.

### *3.4. Dust density*

The dust density distribution can only be constrained from the SED beyond 10 $\mu$m since the matter distribution mainly determines the slope of the redistributed energy by dust emission. We obtain best fits to the *IRAS* data for a simple $r^{-2}$ distribution for a uniform dust flow velocity, whereas a flat distribution of $r^{-1.5}$ is clearly not suitable (Fig. 10). We show that a slightly steeper law of $r^{-2.1}$ neither matches the 60 $\mu$m and 100 $\mu$m fluxes. This result is significant because we compute for the $r^{-2}$ law that the slope is insensitive to the geometrical shell thickness when increased from $10^4$ to $5\,10^4$ times the radius of the inner shell boundary ($R_{\rm c}$). A distribution steeper than unity does not require a cut-off as discussed by Ivezić & Elitzur (1997). The tenuous cold dust tail contributes only slightly to the far-IR fluxes, but when the shell thickness is reduced to a 1000 times $R_{\rm c}$, removing the cooler outer dust envelope, the synthetic 60 $\mu$m and 100 $\mu$m fluxes drop to below the observed

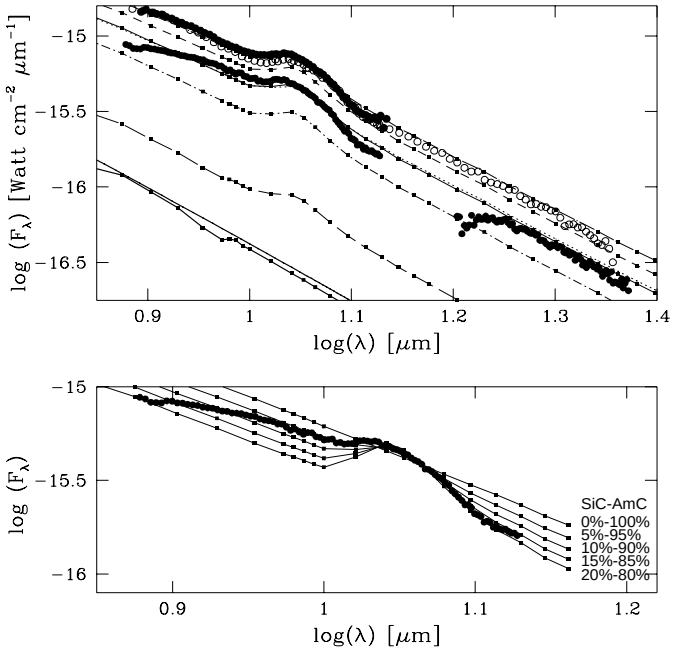


**Fig. 9.** *Upper panel: UKIRT* spectro-photometry of the SiC feature of R For obtained in Jul. '95 (lower dots) and in '93 (upper dots). The latter matches the intensity of the *IRAS* LRS spectrum of '83 (open circles). The reprocessed flux derived for $\tau_{11}$=0.105 (boxed bold line) matches the intensity of the dust emission in '95, together with the coeval optical and near-IR BB photometry of Fig. 8. The model input spectrum with $T_{\rm eff}$=3200 K is shown by the lower bold boxed line with the corresponding blackbody drawn by the solid bold line. The dotted line fits the spectrum of '95 as well, but was computed with a blackbody input model of only 2200 K, without considering the fit to the entire SED. The latter procedure would result in false values for $T_{\rm eff}$ and $\tau_{11}$. *Lower panel:* The shell composition is determined from the shape of the SiC emission, which is best fitted for a mixture of 10% SiC and 90% amorphous carbon. The boxed curves are fits given for mixtures ranging from 0% to 20% SiC

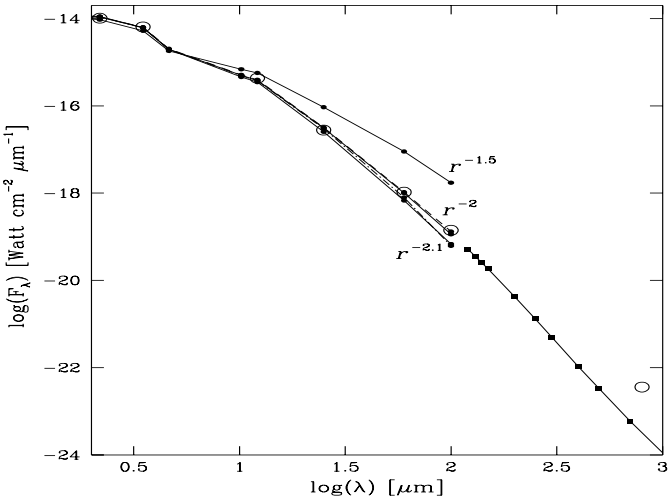


**Fig. 10.** The dust density distribution is strongly constrained to $r^{-2}$ by the slope of the *IRAS* data (open circles). The synthetic BB photometry derived for slightly steeper or flatter power laws does not fit. An increase of the geometrical shell thickness to $5\,10^4\,R_{\rm c}$ preserves the observed slope (upper dashed line), whereas a decrease to $1000\,R_{\rm c}$ underestimates the slope (dash dotted line). The solid boxed line gives the reprocessed spectrum for $r^{-2}$ and $10^4\,R_{\rm c}$, but fails to model the excess observed at 800 $\mu$m (see text)

values. Le Bertre (1997) proposed an improved density law for R For as was approximated by Schutte & Tielens (1989) from dynamical models of Tielens (1983). We found it hard to assess considerable improvement by the latter distribution over the $r^{-2}$-law. These differences are most likely rooted in the higher $T_{\rm eff}$ required for our detailed modelling of the SED of Sept. '95. It should be noted that such smooth density power-laws are clearly unable to model the flux observed by us at 800 $\mu$m with $JCMT$ in Dec. '94 (Bagnulo 1996). Perhaps these sub-mm excess fluxes are related to a-spherical accumulations of cold dust by carbon-rich grain ejection in a preferred direction, possibly from the equator (i.e. forming an equatorial dust torus), as discussed by Whitelock et al. (1997). They compute a distance of 593 pc (or at least half this value) from the Galactic plane which is too large a distance in order to explain the sub-mm excess by emission from IS dust in equilibrium with the IS radiation field. Note further that Le Bertre et al. (1995) have also suggested possible contributions of circumstellar molecular emission to the sub-mm fluxes in the carbon-rich variable GL 3068, after Avery et al. (1992) who estimate these contributions to 70% at 850 $\mu$m for another well-studied carbon star IRC+10216. However, an investigation of the excess flux beyond 100 $\mu$m of R For and other C-stars is outside the scope of our present modelling method which focuses here on the properties near the dust condensation/destruction radius $R_{\rm c}$.

### *3.5. Dust condensation temperature*

The dust condensation temperature $T_{\rm c}$ (assuming identical for amC and SiC) can be fixed from the absolute *IRAS* fluxes and the mid-IR dust emission fluxes. In Fig. 11 it is shown that an increase of $T_{\rm c}$ from 800 K to 1400 K does not affect the descending slope in the IR. Although the determination of this parameter interferes with variations of $T_{\rm eff}$ at these long wavelengths, its value can strongly be constrained from the least-squares method because $T_{\rm eff}$ is strongly constrained by the shape of the entire SED. And as $\tau_{11}$ is strongly fixed by the optical data, the value of $T_{\rm c}$ can accurately be determined because it does not affect the optical fluxes. We find a best fit to the 11.3 $\mu$m feature for 1300$\pm$100 K. The difference with the $T_{\rm c}$ of about 1000 K obtained in Le Bertre (1997) can therefore be attributed to our higher $T_{\rm eff}$ value and the different flux distribution of our input model. Note further that the *UKIRT* spectrum of '93 (and the *IRAS* LRS spectrum) can be well-fitted for $T_{\rm c}$=1000 K (Fig. 11 lower panel, upper open and filled circles), keeping all other parameters held fixed. However, we doubt that this change of $T_{\rm c}$ by 300 K properly reflects a possible physical change of the temperature or density at the dust condensation radius because the changes of $T_{\rm eff}$ and the related changes of the dust optical depth with the stellar variability are not accounted for in the latter fit, as coeval optical data is lacking. The high dust condensation tem-

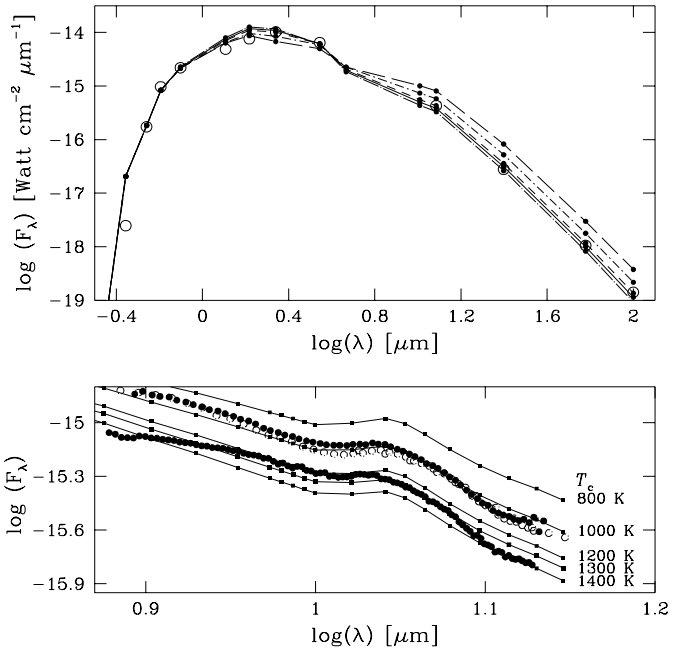


**Fig. 11.** *Upper panel:* The dust condensation temperature is strongly constrained from the *IRAS* data (open circles) because the dust radiates mainly at longer wavelengths. *Lower panel:* An accurate value for $T_c$ ranging between 1200 K and 1300 K is derived from a best fit to the dust emission feature of '95 (lower dots) for $\tau_{11}$=0.105. Other dust emission intensities are also shown by the boxed curves computed for $T_c$=800 K, 1000 K and 1400 K

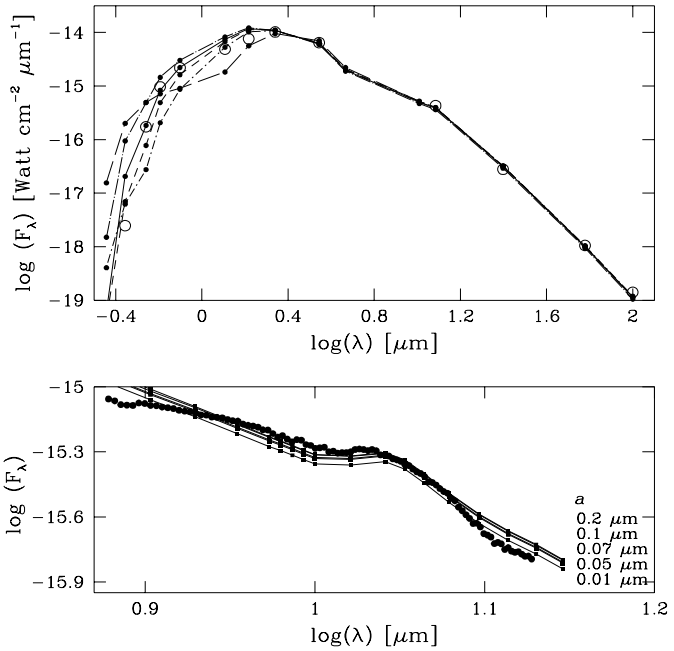


**Fig. 12.** *Upper panel:* The grain radius is strongly constrained by the optical BB data (open circles). A best fit is derived for single-grain radii between 0.05 $\mu$m (bold curve) and 0.07 $\mu$m (short-dashed curve). Scattering by the dust remains negligible for $a \leq 0.2\,\mu$m (long-dashed curve) because R For is too faint toward shorter wavelengths. The other curves are computed for $a$=0.01 $\mu$m (long-dash dotted) and 0.1 $\mu$m (short-dash dotted). *Lower panel:* As the shell optical depth at 11.3 $\mu$m is rather small an increase of the grain radius from 0.01 $\mu$m to 0.2 $\mu$m results in minor increases of the dust emission flux levels

perature derived by us confirms the value of 1300 K obtained for IRC+10216 by Danchi et al. (1990). In a recent study of properties of dust shells around carbon Mira variables Groenewegen et al. (1998) also obtained $T_c$=1300 K for R For, although their radiative transfer calculations just assume an input blackbody of only 2300 K and the BB photometric data and mid-IR spectra are not coeval. They compute values for SiC/amC of 0.04 and $\tau_{11.33}$=0.12, in fine agreement with our result of 10% SiC and $\tau_{11}$=0.105. Our method however selects a synthetic stellar model spectrum with considerably higher $T_{\rm eff}$=3200 K, whereas their blackbody input distribution overestimates the optical BB photometry, also found by Le Bertre (1997). As our synthetic BB photometry accounts for the optical molecular opacities we can further constrain the grain radius by accurate SED fits to the shorter wavelengths.

### *3.6. Grain radius*

The dust grain radius is chiefly constrained from the optical data. In Fig. 12 we compute the SED for single grain radii with $0.01\,\mu\text{m} \leq a \leq 0.2\,\mu$m, treated as homogeneous spheres. A best fit to the *BVRI* data constrains their sizes between 0.05 $\mu$m and 0.07 $\mu$m and also properly fits the SiC feature (Fig. 12 lower panel). As the grain radius is increased, more optical light is absorbed and redistributed to the longer wavelengths. But for grain radii larger than 2000 Å the scattering of stellar optical radiation by the circumstellar dust cloud into the line of sight increases strongly, particularly for larger optical depths which sample the denser and hotter inner portion of the shell. However, for R For the dust scattering is rather small as the average grain size remains below 0.1 $\mu$m and the central star is too faint at shorter wavelengths. Further best-fit calculations with grain size power-law distributions of the form $n(a) \propto a^{-q}$, having sharp boundaries at $0.01\,\mu\text{m} \leq a \leq 0.25\,\mu$m, favour rather high $q$ values between 3.5 and 4.5. From this steep drop-off in grain size we integrate that only 1.7 percent of the total dust particle number may contain grains with radii larger than 0.05 $\mu$m in the tenuous outer layers. This result confirms SED modelling studies by Griffin (1990) and by Bagnulo et al. (1995) for IRC+10216. Note that Jura et al. (1997) found that for amorphous carbon grains around this object about 1% of the mass must contain particles that are larger than 0.05 $\mu$m in radius in order to explain the observed circumstellar polarisation.

## 4. Dynamic modelling

Measurements of the half width at zero intensity of the rotational CO (J=1-0) millimetre emission lines give values ranging from 16 to 20 $\text{km}\,\text{s}^{-1}$ for the gas expansion velocity of the circumstellar envelope of R For, yielding an estimate for the gas mass loss rate of 1.2 to $3.4\,10^{-6}\,M_\odot\,\text{y}^{-1}$ (Olofsson et al. 1988, 1993; Loup et al. 1993). Note that these values are likely to be systematically overestimated, as they are derived for optically thick

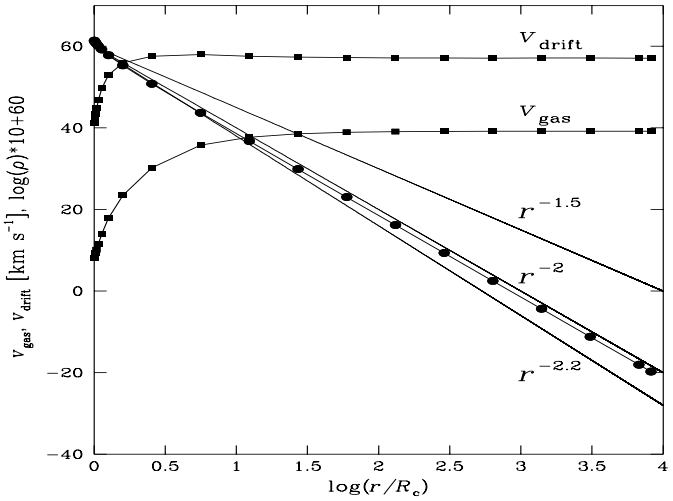


**Fig. 13.** When including radiation pressure on the dust shell the computed density profile (solid line with filled circles) matches an $r^{-2}$-law. Other power-laws are shown for $r^{-1.5}$ and $r^{-2.2}$. The gas outflow velocity increases from 8 km s$^{-1}$ at $R_{\rm c}$ to the terminal velocity of 39 km s$^{-1}$, whereas the dust drift velocity increases from 42 to 57 km s$^{-1}$ (boxed curves)

shells (Knapp & Morris 1985, Loup et al. 1993), whereas the circumstellar dust shell (CDS) of R For is rather optically thin. The variable P-Cygni profiles of the K I line at 7699 Å and the variable H$\alpha$ emission displaying blue-shifts above 10 km s$^{-1}$ (Barnbaum & Morris 1993) may indicate variable mass-loss rates from the stellar surface.

### *4.1. Mass-loss rate and terminal velocity*

Gas mass-loss rates can be derived via dynamical modelling of the SED. Three forces act on a dust grain in the CDS: the radiation pressure, the gravitational pull of the star and the drag force of the gas (Netzer & Elitzur 1993). When these forces are included in the equation of motion and coupled to the radiative transfer, the importance of radiation pressure on grains driving the envelope expansion can be evaluated. In this 'full dynamic' calculation the dust density structure follows from the momentum transfer between radiation and dust, whereas the steady-wind solution of Sect. 3 requires an a priori knowledge of the density profile which permits to neglect this transfer. As the density profile is constrained by the *IRAS* BB photometry and adopts a gradient of $r^{-2}$, the other shell parameters are well determined and applicable in the full dynamical treatment where $T_{\rm eff}$ and the shell optical depth are varied with stellar pulsation. The dust condensation temperature is fixed at 1300 K and $a$ is set to 0.05 $\mu$m because multi-grain sizes result in a range of dust drift velocities which we currently do not consider. In Fig. 13 we show that the density gradient computed from these parameters strongly matches the $r^{-2}$ law as found before from the steady-state fit.

In Table 1 we list the parameters of the models with the same optical depth as those shown in Fig. 8. Columns 1–6 give the stellar effective temperature, the optical depths at 11 and 1 $\mu$m, the dust condensation radius, the gas mass-loss rate, and its terminal velocity $V_\infty$. Column 7 lists an upper value on the stellar mass below which the effect of gravity is negligible and the computed density profile remains independent of $M_*$. The values for gas mass-loss rate and velocity are derived for the canonical gas-to-dust mass ratio of $r_{\rm gd}$=200 and a dust grain bulk density of $\rho_{\rm s}$=2 g cm$^{-3}$. The latter value has been computed on the basis of an estimate of $\rho_{\rm s}$=1.85 g cm$^{-3}$ (Rouleau & Martin 1991) for a mixture of 90% amC and of 3.2 g cm$^{-3}$ (Pégourié 1988) for 10% SiC grains. Note that the computed mass-loss rates scale with $(r_{\rm gd}\rho_{\rm s})^{1/2}$ and thus the outflow velocity with $(r_{\rm gd}\rho_{\rm s})^{-1/2}$. The dust mass loss rate derived from our best fit equals $1.5\,10^{-8}\,M_\odot\,{\rm y}^{-1}$, which is about three times larger than the value estimated by Groenewegen et al. (1998) of $5.1\,10^{-9}\,M_\odot\,{\rm y}^{-1}$. This difference can only partially be ascribed to the different estimates of the stellar distance. We have adopted a stellar luminosity of $10000\,L_\odot$ for a distance of 0.93 kpc (Sect. 3.2), whereas Groenewegen et al. (1998) adopted $5790\,L_\odot$ and 0.64 kpc. For a steady-state wind without radiation pressure, the dust mass-loss rate scales linearly with distance (Bagnulo et al. 1997), which can therefore not account for this difference. We presume that it results from differences in the overall applied method, in particular by the low $T_{\rm eff}$=2300 K they adopted.

**Table 1.** Gas mass-loss rate and terminal velocity computed by radiation pressure on the dust envelope for the models of Fig. 8. The parameters of the fits to the SED in the phase of maximum light of Jan. '96 are also given

| $T_{\rm eff}$ (K) | $\tau_{11}$ 11 $\mu$m | $\tau_1$ 1 $\mu$m | $R_{\rm c}$ (cm) | $\dot{M}$ ($M_\odot$ y$^{-1}$) | $V_\infty$ (km s$^{-1}$) | $M_*^{\leq}$ ($M_\odot$) |
|---|---|---|---|---|---|---|
| Sept. '95 | | | | | | |
| 3200 | 0.010 | 0.18 | $1.24\,10^{14}$ | $0.55\,10^{-6}$ | 36.7 | 0.8 |
| 3200 | 0.057 | 1.05 | $1.32\,10^{14}$ | $2.02\,10^{-6}$ | 40.4 | 1.5 |
| 3200 | 0.105 | 1.91 | $1.37\,10^{14}$ | $3.01\,10^{-6}$ | 39.2 | 1.8 |
| 3200 | 0.153 | 2.78 | $1.42\,10^{14}$ | $3.86\,10^{-6}$ | 36.4 | 1.9 |
| 3200 | 0.200 | 3.64 | $1.46\,10^{14}$ | $4.66\,10^{-6}$ | 34.5 | 1.9 |
| Jan. '96 | | | | | | |
| 3200 | 0.070 | 1.27 | $1.33\,10^{14}$ | $2.28\,10^{-6}$ | 41.3 | 1.6 |
| 3500 | 0.092 | 1.69 | $1.50\,10^{14}$ | $3.03\,10^{-6}$ | 38.9 | 2.0 |

In Fig. 13 we show that the dust drift velocity $v_{\rm drift}$=$v_{\rm dust} - v_{\rm gas}$ increases to $\sim$57 km s$^{-1}$ moving outward, resulting in a relative decrease of the dust opacity. At $R_{\rm c}$ the radiative force causes dust flow velocities up to 6 times larger than the local gas velocity, levelling off to about a factor 2 in the outer dust envelope. Note that Netzer & Elitzur (1993) found $v_{\rm d}$ values exceeding 100 km s$^{-1}$ in luminous carbon stars (when including scattering) for grain sizes of $\sim$0.5 $\mu$m. We find for R For that the radiation pressure on dust is by far sufficient to provide the momentum which drags the gas along in order to model the CO line width. This is however valid when only the stellar mass is limited by $\simeq 2\,M_\odot$, otherwise the role of mechanical momentum sources has to be considered as well in order to overcome the gravitational pull. When assuming that the star is surrounded by

**Table 2.** Near-IR magnitudes on the raising branch of the light curve of R For observed at *SAAO* (excerpt from Table 2 of Whitelock et al. (1997)). The data of Sept. 6 was obtained by us at *CST* and is presently modelled in conjunction with coeval optical BB photometry and mid-IR spectroscopy

| date | Jul. date 2440000+ | $J$ | $H$ | $K$ (mag.) | $L$ |
|---|---|---|---|---|---|
| Aug. 02 1995 | 9932.7 | 4.82 | 3.03 | 1.65 | 0.17 |
| Aug. 18 1995 | 9948.6 | 4.84 | 3.03 | 1.65 | 0.22 |
| Sept. 06 1995 | 9967.7 | 4.49 | 2.92 | 1.55 | 0.07 ($L'$) |
| Sept. 14 1995 | 9975.5 | 4.76 | 2.98 | 1.61 | 0.14 |
| Oct. 10 1995 | 10001.5 | 4.68 | 2.90 | 1.54 | 0.14 |
| Nov. 12 1995 | 10034.4 | 4.46 | 2.73 | 1.42 | 0.01 |
| Dec. 05 1995 | 10057.3 | 4.14 | 2.47 | 1.23 | -0.16 |
| Jan. 05 1996 | 10088.3 | 3.81 | 2.20 | 1.02 | -0.34 |
| Jan. 28 1996 | 10111.3 | 3.66 | 2.05 | 0.92 | -0.42 |

a spherical symmetric dust envelope we compute a distance to the point of dust condensation of $R_{\rm c}$=3.7 to 4.9 times the stellar radius of about 400 to 500 $R_{\odot}$. The time-dependent hydrodynamical treatment of levitation of LPV and Mira atmospheres by pulsation in order to provide sufficient gas density beyond $R_{\rm c}$ is discussed by i.e. Fleischer et al. (1992) or Bowen (1988). We presently limit our modelling of R For to the effect of the variable radiation field with stellar pulsation on the conditions in the CDS as inferred from its variable SED.

### *4.2. SED variability in '95*

Whitelock et al. (1997) observed an increase of the $J$, $H$, $K$ and $L$ magnitude after Sept. 14 '95 over a period of 136 days as listed in Table 2. If we increase $T_{\rm eff}$ of the input model from 3200 K to 3700 K, for $\tau_{11}$=0.105 and keeping all other shell parameters held fixed, we compute that the synthetic $U$, $B$, $V$, $R$, $I$ magnitudes increase by $1^{\rm m}.65$, $1^{\rm m}.21$, $0^{\rm m}.89$, $0^{\rm m}.56$, $0^{\rm m}.30$ resp., but the synthetic $J$, $H$ and $K$ magnitudes *decrease* by $0^{\rm m}.03$, $0^{\rm m}.19$, $0^{\rm m}.11$. These opposite changes are shown in Fig. 14 for the smoothed input spectra and their reprocessed SEDs in a magnitude scale. It results from the input spectra crossing over near log($\lambda$)=0.1 $\mu$m which produces reduced flux levels in the near-IR. As the optical and near-IR photometry are observed to vary *in phase* with decreasing amplitudes toward longer wavelengths (but note also that small phase lags in the light curves are observed), we conclude that *the entire SED variability cannot be modelled from changes of* $T_{\rm eff}$ *alone*.

These opposite changes of the optical and the near-IR amplitudes can be circumvented by changing the shell optical depth in conjunction with $T_{\rm eff}$. In Fig. 8 we have shown that these fluxes alter *in phase* when $\tau_{11}$ is varied between 0.01 and 0.2. By lowering $\tau_{11}$ from 0.105 to 0.05 (at 3200 K) the dynamical calculation yields an increase in the synthetic $U$ magnitude of $3^{\rm m}.61$, $2^{\rm m}.26$ ($B$), $1^{\rm m}.73$ ($V$), $1^{\rm m}.27$ ($R$), $0^{\rm m}.94$ ($I$), $0^{\rm m}.49$ ($J$), $0^{\rm m}.26$ ($H$) and $0^{\rm m}.03$ in $K$. The mid- and far-IR amplitudes however still decrease because the SEDs for various $\tau_{11}$ cross-over between the $K$ and $L'$ band.

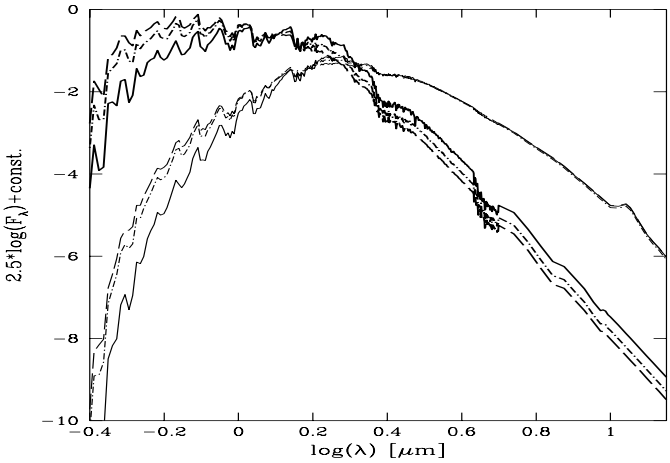


**Fig. 14.** The input model spectra (bold curves) are reprocessed by the CDS for $T_{\rm eff}$=3200 K (solid curves) in the variability phase of Sept. '95 and for the phase of maximum light of Jan. '96 with $T_{\rm eff}$=3500 K (dash dotted curves) and 3700 K (dashed curves). The optical depth of the CDS is fixed at $\tau_{11}$=0.105

The large amplitude observed in $V$ strongly constrains the range of both parameters by fitting the phase of maximum light (JD 2450111, Table 2). A reliable estimate of $\triangle V$ (up to the phase of maximum light) is obtained from the amplitude on the raising branch observed by AAVSO three pulsation cycles earlier (e.g. Battrick & Wapstra, eds., 1997 in The HIPPARCOS Catalogue - Light Curves, HIP 011582). During this period from JD 2448074 - JD 2448197 Whitelock et al. (1997) measured an increase of $J$ by $1^{\rm m}.21$ which compares to the increase of $J$ by $1^{\rm m}.16$ they have observed during the 179 days from minimum to maximum light during the phase we presently model. The good coverage of the AAVSO light curve yields a $\triangle V$ of $2^{\rm m}.2$, which corresponds with an increase of $V$ by $1^{\rm m}.6$-$1^{\rm m}.7$ after our photometric and spectroscopic observations of Sept. '95. When integrating the SED at the phase of maximum light (Jan. 28 '96) we derive for the observed bolometric flux $6.1\ 10^{-7}$ erg s$^{-1}$ cm$^{-2}$. It corresponds to an increase of the bolometric flux of about 60% since Sept. '95 (with $F_{\rm bol}$=3.8 $10^{-7}$ erg s$^{-1}$ cm$^{-2}$), resulting from the changing stellar angular diameter and changes of the $T_{\rm eff}$. Note that the SEDs in Fig. 14 are scaled according to these observed $F_{\rm bol}$ values for both phases.

In Fig. 15 we show that good fits to the $V$, $J$ and $H$ maxima are derived for ($T_{\rm eff}$, $\tau_{11}$)=(3200, 0.07) or (3500, 0.09). We can interpret this decrease of the optical depth of the CDS as being caused by the raise of $T_{\rm eff}$. In Table 1 we compute that an increase of 300 K enlarges the dust condensation radius $R_{\rm c}$ from 1.37 $10^{14}$ cm to 1.5 $10^{14}$ cm and as dust then forms farther out in the wind at lower density, the overall dust density of the shell diminishes and hence its optical depth. However, we show in Fig. 15 that the amplitudes observed in the $K$ and $L$ band cannot be modelled together with the amplitudes observed at shorter wavelengths by varying $\tau$ and $T_{\rm eff}$. We find that changes of the dust properties can neither account for this discrepancy. A strong reduction of the grain radius to $a$=0.001 $\mu$m increases the optical fluxes but leaves the $K$ and $L'$ magnitudes practi-

cally invariable. An increase of $T_c$ to the dust nucleation limit of 1500 K also produces changes which are rather marginal at these wavelengths. The same follows from varying the dust composition, which is moreover unlikely as the weak SiC emission of R For displays an invariable shape. We therefore think that the failure of modelling the $K$ and $L$ amplitudes originates in the time-independence of the smooth shell density structure we presently consider in our models.

In a time-dependent hydrodynamic modelling Winters et al. (1994) computed near-IR light curves of R For which match the observed amplitudes. Their models reveal a multi-periodic formation of new discrete dust layers around minimum light at the inner dust envelope where grains can form at low temperature and grow by compression of pulsation density waves while driven outward by radiation pressure. These models also explain the systematic drift in magnitude observed in these bands. Detailed radiative transport calculations through an expanding onion-like density structure of the CDS is outside the scope of our present modelling from synthetic input spectra. However, our assumption of an (average) radially monotonic decreasing density profile shows already that the optical amplitudes and $J$ and $H$ amplitudes are mainly affected by small changes of $T_{\rm eff}$ with pulsation and of the dust optical depth. When neglecting the hydrodynamic contribution in the momentum equation for the radiative driving of the outer dust envelope we compute (Table 1) that the changes of the stellar input spectrum between minimum and maximum light hardly affect the mass-loss rate ($\triangle \dot{M} \leq 1\%$) and that the terminal velocity remains practically constant ($\triangle V_\infty \leq 2\,{\rm km\,s^{-1}}$).

## 5. Conclusions

$i$. We have modelled the circumstellar environment of the notorious carbon Mira R For for a pulsation phase in Sept. '95. To this end we have developed a new modelling method which accurately determines the conditions of the CDS and the $T_{\rm eff}$ of the central source. Therefore our method requires coeval BB optical and near-IR photometry in conjunction with spectra of mid-IR dust emission. This precise modelling of the observed SED is achieved by means of detailed stellar model spectra which are reprocessed through the dusty envelope and from which we compute 'synthetic' BB photometry. The $T_{\rm eff}$ of the input spectrum is therefore determined from a comparison with observed optical spectra.

$ii$. Since our method properly accounts for molecular opacity sources, the SED of R For at shorter wavelengths reveals that the star has $T_{\rm eff} \simeq 3200\,{\rm K}$ and is surrounded by a rather optically thin dust shell with a mean grain radius of 0.05 $\mu$m and mainly composed of 'warm' amorphous carbon and only 10% SiC with $T_{\rm c} \simeq 1300\,{\rm K}$. The density structure of the outer envelope assumes a $r^{-2}$ gradient by radiation pressure onto dust. When $M_* \leq 2\,M_\odot$ this pressure provides sufficient drag momentum to model the observed envelope expansion velocity with a gas mass-loss rate of 3–4 $10^{-6}\ M_\odot\,{\rm y^{-1}}$.

$iii$. The modelling of the SED variability of R For shows that the amplitudes of the optical and near-IR light curves are strongly affected by changes of $T_{\rm eff}$ of only a few hundred degrees and by subsequent small variations of the shell optical depth. The near-IR $K$ and $L$ amplitudes can however not be modelled in conjunction with the optical light curves by changes of these model parameters or by changes of the dust properties. We conclude therefore that these fluxes may also be affected by density variations with pulsation at the inner radius of the dust envelope.

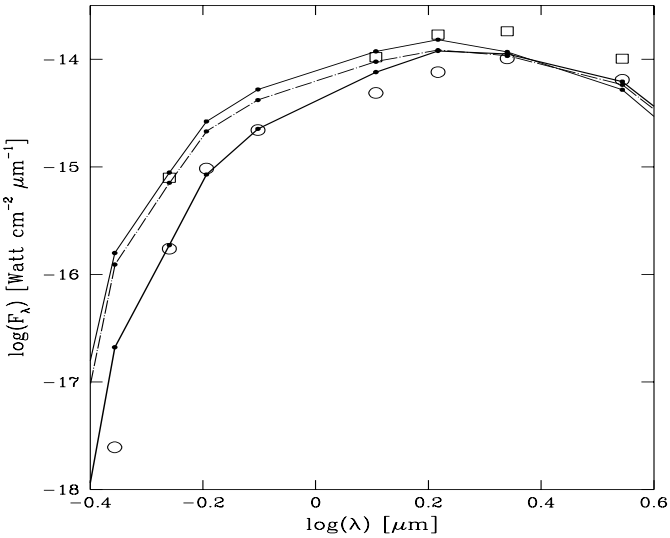


**Fig. 15.** Variability of the optical and near-IR SED of R For between Sept. '95 (open circles) and maximum light (boxes) of Table 1. The best fit (bold line) to the SED of Sept. '95 is obtained for $T_{\rm eff}$=3200 K and $\tau_{11}$=0.105. The maximum phase is best fitted for (3200, 0.07) (thin solid line) or (3500, 0.09) (dash-dotted line)

We plan to model the SED variability of $o$ Cet (Mira) from stellar input spectra with time-dependent hydrodynamic models of density waves in the CDS. The newly presented method will serve next to investigate possible changes of the dust properties from the recently observed changes of the shape of the silicate feature.

*Acknowledgements.* The authors are grateful to Dr. C. Barnbaum for providing us with high resolution spectra of R For. A.L. would like to thank Drs. D. Andrews, F. Byrne and R.D. Cannon for providing him with high-quality AAO spectra of C-stars and Dr. D. Kilkenny for information on the calibration of the optical photometry. The authors thank Dr. P. Hauschildt for invaluable information on the provided input model grid for M-S-C giants. The authors are grateful to Dr. T. Tsuji for useful comments on an early version of this paper and discussion about this research. This work was carried out under PPARC grant L21259. SB has been supported by the Austrian *Fonds zur Förderung der Wissenschaftlichen Forschung*, project P12101-AST. Research at Armagh Observatory is grant-aided by the Department of Education for N. Ireland, while partial support is provided in terms of both software and hardware by the STARLINK Project which is funded by the UK PPARC. The UKIRT is operated by the Joint Astronomy Centre on behalf of PPARC.

## References

Alksne Z.K, Ikaunieks Ya.Ya., 1981, J.H. Baumert (ed.) Carbon Stars. Astronomy and Astrophysics Series Vol. 11, Chapter 4, Pachart Publ. House, Tucson, USA

Allard F., Hauschildt P.H., 1995, ApJ 445, 433
Allard F., Lawlor T., Alexander D.R., Hauschildt P.H., 1995, BAAS 187, 103.11
Alonso A., Arribas S., Martinez-Roger C., 1994, A&AS 107, 365
Avery L.W., Amano T., Bell M.B., 1992, ApJS 83, 363
Bagnulo S., 1996, Modelling of Circumstellar Environments around Carbon- and Oxygen-Rich Stars. Ph.D. dissertation, Queen's University Belfast, N. Ireland, p. 116
Bagnulo S., Doyle J.G., Griffin I.P., 1995, A&A 301, 501
Bagnulo S., Doyle J.G., Skinner C.J., Camphens M., 1997, A&A 321, 605
Bagnulo S., Doyle J.G., Andretta V., 1998, MNRAS 296, 545
Barnbaum C., 1994, ApJSS 90, 317
Barnbaum C., Morris M., 1993, In: Schwarz H.E. (ed.) Proceedings of the Second ESO/CTIO Workshop: Mass Loss on the AGB and Beyond. ESO, Garching, p. 280
Barnbaum C., Stone R.P.S., Keenan P.C., 1996, ApJS 105, 419
Barthès D., Chenevez J., Mattei J.A., 1996, AJ 111, No. 6, 2391
Battrick B., Wapstra H. (eds.), 1997, In: The HIPPARCOS and TYCHO Catalogues. Hipparcos Variability Annex: Light Curves, SP1200 - Vol. 12, ESA Publications Division, Noordwijk, The Netherlands
Bowen G.H., 1988, ApJ 329, 299
Cohen M., 1979, MNRAS 186, 837
Danchi W.C., Bester M., Degiacomi C.G., McCullough P.R., Townes C.H., 1990, ApJ 359, L59
Feast M.W., Whitelock P.A., Catchpole R.M., Roberts G., Overbeek M.D., 1984, MNRAS 211, 331
Feast M.W., Whitelock P.A., Carter B.S., 1990, MNRAS 247, 227
Fleischer A.J., Gauger A., Sedlmayr E., 1992, A&A 266, 321
Griffin I.P., 1990, MNRAS 247, 591
Groenewegen M.A.T., Whitelock P.A., Smith C.H., Kerschbaum F., 1998, MNRAS 293, 18
Hanner M.S., 1988, Infrared Observations of Comets Halley and Wilson and Properties of the Grains (NASA89-13330), 22
Hauschildt P.H., Baron E., Allard F., 1997, ApJ 488, 428
Haisch B.M., 1979, A&A 72, 161
Ivezić Z., Elitzur M., 1995, ApJ 445, 414
Ivezić Z., Elitzur M., 1997, MNRAS 287, 799
Ivezić Z., Nenkova M., Elitzur M., 1996, User Manual for DUSTY, 1st draft, available on Internet
Ivezić Z., Groenewegen M.A.T., Men'shchikov A., Szczerba R., 1997, MNRAS 291, 121
Jura M., Turner J., Balm S.P., 1997, ApJ 474, 741
Knapp G.R., Morris M., 1985, ApJ 292, 640
Landolt-Börnstein, 1982, In: Schaifers K., Voigt H.H. (eds.) Numerical Data and Functional Relationships in Science and Technology, Vol. 2b. Stars and Star Clusters. Springer, New York, p. 71
Le Bertre T., 1988, A&A 190, 79
Le Bertre T., 1992, A&AS 94, 377
Le Bertre T., 1997, A&A 324, 1059
Le Bertre T., Gougeon S., Le Sidaner P., 1995, A&A 299, 791
Little-Marenin I.R., Little S.J., 1988, ApJ 333, 305
Loup C., Forveille T., Omont A., Paul J.F., 1993, A&AS 99, 291
Milne D.K., Aller L.J., 1980, AJ 85, 17
Monnier J.D., Geballe T.R., Danchi W.C., 1998, ApJ 502, 833
Netzer N., Elitzur M., 1993, ApJ 410, 701
Olofsson H., Eriksson K., Gustafsson B., 1988, A&A 196, L1
Olofsson H., Eriksson K., Gustafsson B., Calström U., 1993, ApJS 87, 267
Pégourié B., 1988, A&A 194, 335
Rouleau F., Martin P.G., 1991, ApJ 377, 526
Schutte W.A., Tielens A.G.G.M., 1989, ApJ 343, 369
Speck A.K., Barlow M.J., Skinner C.J., 1997, MNRAS 288, 431
Tielens A.G.G.M., 1983, ApJ 271, 702
Treffers R., Cohen M., 1974, ApJ 188, 545
Whitelock P.A., 1997, In: Wing R.F. (ed.) Proc. IAU Symp. 177, The Carbon Star Phenomenon. Kluwer, Dordrecht
Whitelock P.A., Feast M.W., Marang F., Overbeek M.D., 1997, MNRAS 288, 512
Winters J.M., Fleischer A.J., Gauger A., Sedlmayr E., 1994, A&A 290, 623
Zubko V.G., Mennella V., Colangeli L., Bussoletti E., 1996, MNRAS 282, 1321